Supporting Information

Louvi et al. 10.1073/pnas.1012617108

SI Materials and Methods

Mice. All mice were maintained in compliance with National Institutes of Health guidelines and approval of the Yale University Institutional Animal Care and Use Committee. *Cerebral cavernous malformation 3* ($Ccm3^{lox}$) has been described (1); *Gfap*-Cre (2), *Nestin*-Cre (3), and *Emx1*-internal ribosome entry site (IRES)-Cre (4) mice were obtained from JAX. All mice were maintained in mixed genetic background (C57BL6, 129, and FVB).

Generation of the Ccm3 conditional allele. The targeting strategy has been reported elsewhere (1). Briefly, we designed a construct to introduce loxP sites flanking exons 4 and 5 of *Ccm3* using the pEASYflox backbone. Transfected 129/C57BL/6 ES cells were screened for correct integration of the targeting vector by PCR and Southern blot analysis. Two independent ES clones were injected into blastocysts and founders transmitting the $Ccm3^{lox}$ allele to their progeny were obtained. Mouse genotypes were determined by PCR using allele-specific primers (5′-CTCAGTGTAGTCATGAAAAGAGT-3′ and 5′-CCAGCATCCTTTGCCTCTCC-3′), which amplify fragments of 103 and 151 bp from the WT and floxed alleles, respectively.

Cre lines.

i) *Nestin*-Cre (JAX stock number 003771) (3). In this transgenic line, Cre is expressed under the control of the rat *nestin* promoter and nervous system-specific enhancer in neuronal progenitors by embryonic day (E) 11 (3). Although the *Nestin-Ccm3* mutants were not analyzed further, they differ from previously reported and apparently normal *Nestin-Ccm3* mutants lacking any neural phenotype (1). We note that the *Nestin-Cre* driver used in our study directs recombination earlier and in a broader domain of the embryonic central nervous system (CNS), indicating that neural progenitors might have different temporal requirements for *Ccm3* during development. The *Nestin*-Cre driver resulting in viable and apparently normal *Nestin-Ccm3* animals has a later onset of recombination (5), which is initiated in the midbrain and hindbrain around E10.5, but it is only detected in the forebrain by E14.5 and is, in addition, mosaic (5).

ii) *Gfap*-Cre (JAX stock number 004600) (2). In this transgenic line, Cre is expressed under the control of the human *Gfap* promoter. Cre-mediated recombination occurs primarily in the CNS. Cre is active in most dorsal telencephalic radial glia and their progeny, including neurons, astrocytes, oligodendroglia, and ependymal cells lining the ventricular system (6). Developmental onset of transgenic expression occurs in the dorsomedial telencephalon by E13.5 and becomes nearly uniform throughout the CNS, including the cerebellum, by birth (2, 6). This is a widely used Cre driver, with exceptionally faithful recombination characteristics, that is not active in endothelial cells (7) and is lacking aberrant ectopic recombination activity (8).

iii) *Emx1*-IRES-Cre (JAX stock number 005628) (4). In this knock-in line generated by homologous recombination, *Cre* was inserted into the 3′ UTR of the *Emx1* locus and is expressed from the endogenous locus. *Cre*-mediated recombination begins at E9.5 in dorsomedial telencephalon, expands to the entire forebrain and hippocampal primordia by E11.5, encompasses all proliferating and postmitotic cells by E12.5, and affects the majority (~90%) of neurons in the neocortex and hippocampus as well as cortical glia, including astrocytes and oligodendrocytes; neither are blood vessels derived from *Emx1*-expressing precursors nor is *Emx1*-Cre activity detected in adult neocortical vessels (4).

Crosses. Cre mice were first mated with $Ccm3^{lox/lox}$ mice to generate Cre^{+};$Ccm3^{lox/+}$ mice. *Gfap*-Cre;$Ccm3^{lox/+}$, *Nestin*-Cre;$Ccm3^{lox/+}$, or *Emx1*-Cre;$Ccm3^{lox/+}$ mice were crossed with $Ccm3^{lox/lox}$ mice. The resulting mutant progeny (*Nestin-Ccm3*, *Gfap-Ccm3*, and *Emx1-Ccm3*) is hemizygous for the respective *Cre* allele and homozygous for the $Ccm3^{lox}$ allele, whereas littermate controls are hemizygous for the *Cre* allele and carry one $Ccm3^{lox}$ allele or carry two $Ccm3^{lox}$ alleles but not *Cre* (the phenotypes of all types of control animals are indistinguishable from WT in all three crosses). Multiple breeding pairs were set up for each cross type, and all animals analyzed were progeny of Cre^{+};$Ccm3^{lox/+}$ (x) $Ccm3^{lox/lox}$ parents. Mice were genotyped using PCR primers for *Ccm3* (see above) and *Cre* (5′-CCGGGCTGCCACGACCAA-3′ and 5′-GGCGCGGCAACACCATTTTT-3′).

Recombination of the floxed allele. In mutant animals, we determined the expression of *Ccm3* mRNA by in situ hybridization of brain sections (Fig. S1 *A* and *B*). Compared with controls, *Ccm3* was significantly down-regulated in mutant mice. Similarly, Western blot analysis of protein lysates from whole brain or cortical astrocytes (Fig. 2 and Fig. S1*C*) indicated that CCM3 protein levels were significantly down-regulated compared with controls. Importantly, both at the mRNA and protein levels, CCM3 expression was retained in nonneural cells in all three conditional mutants (Fig. S1).

In Situ Hybridization. Mice were anesthetized using injectable anesthetics (100 mg/kg ketamine and 10 mg/kg xylazine) and perfused intracardially with 4% paraformaldehyde (PFA). Brains were removed, postfixed overnight in 30% sucrose in 4% PFA, and sectioned in the coronal plane on a Leica sledge cryomicrotome at 36 μm (Leica Microsystems). Sections were mounted on slides and processed for nonradioactive in situ hybridization as described previously (9). RNA probes complementary to mouse *Ccm3*, *collagen 4a1*, *connexin 43*, *Gfap*, and *vimentin* were prepared and labeled with digoxigenin-11-UTP. Sections were analyzed using a Zeiss Stemi dissecting microscope or a Zeiss AxioImager (Zeiss) fitted with an AxioCam MRc5 digital camera. Images were captured using AxioVision software (Zeiss) and assembled in Adobe Photoshop.

Immunohistochemistry. Mouse brains were collected and fixed as described above, cryoprotected in 30% sucrose in PBS, sectioned at 40 μm using a sledge cryomicrotome (Leica) in the coronal plane, and processed free-floating. For diaminobenzidine (DAB) staining, sections were treated with 1% H_2O_2, washed in PBS, and preincubated in blocking solution (BS) containing 5% normal donkey serum (Jackson ImmunoResearch Laboratories), 1% BSA, 0.1% glycine, 0.1% L-lysine, and 0.03% Triton-X-100. The sections were then incubated with primary antibodies for 48 h at 4 °C. After washes with PBS, the sections were incubated with secondary antibodies (raised in donkey, 1:250 dilution; Jackson ImmunoResearch Laboratories) for 2 h at room temperature, washed in PBS, and then incubated with Vectastain ABC Elite solution (Vector Laboratories) for 2 h. Sections were developed using the DAB substrate kit for Peroxidase (Vector), then rinsed, mounted onto glass slides, allowed to dry, dehydrated, and cover-slipped. For immunofluorescence, the H_2O_2 step was omitted; secondary antibodies were Alexa-Fluor–con-

jugated (1:500 dilution; Molecular Probes), and the sections were cover-slipped with DAPI-containing Vectastain (Vector).

Antibodies. We used primary antibodies against the following antigens: PECAM 1 (1:50, #CBL1337; Chemicon; #sc-18916; Santa Cruz Biotechnology), GFAP (1:1,000, #31223; Advanced Immunochemical; 1:100, #G3839; Sigma-Aldrich), Ccm3 (1:1,000, #sc-67907 and #sc-67908; Santa Cruz Biotechnology), Ccm3 (1:200 for immunohistochemical staining of lesions; provided by Wang Min, Yale School of Medicine, New Haven, CT) (1), caspase 3 (1:1,000, #9662; Cell Signaling Technology), cleaved caspase 3 (Asp175; 1:1,000, #9661; Cell Signaling Technology), β-actin (1:1,000, A-2066; Sigma-Aldrich), vascular endothelial (VE)-cadherin (1:200, #sc-6458; Santa Cruz Biotechnology), Akt (1:1,000, #4691; Cell Signaling Technology), phosphorylated Akt (pAkt; Ser473; 1:1,000: Western blot (WB), 1:100: immunohistochemistry (IHC), #4058; Cell Signaling Technology), pAkt; Thr308; 1:1,000: WB, 1:100: IHC, #4056; Cell Signaling Technology) GAPDH (1:1,000, #sc-25778; Santa Cruz Biotechnology), FoxO1 (1:1,000, #9454; Cell Signaling Technology), phosphorylated FoxO1 (pFoxO1; Ser256; 1:1,000, #9465; Cell Signaling Technology), and Angiopoietin 1 (Ang1; 1:500, #ab8451; Abcam).

NADPH-Diaphorase Histochemistry. Brains were fixed by perfusing animals with 4% PFA; sections (40–50 μm), prepared as above, were incubated in 0.25 mg/mL NADPH-diaphorase (Sigma) diluted in PBS/1.25% vol/vol Triton X-100 containing 0.35 mg/mL nitro blue tetrazolium chloride (NBT) for 45–60 min at 37 °C.

BrdU Labeling. For labeling of dividing cells at embryonic stages, pregnant females were injected intraperitoneally with a solution of BrdU (15 mg/mL in saline) at 20 mg/g body weight. BrdU incorporation was detected with anti–BrdU-FITC antibody (Beckton-Dickinson) as described (10). Adult brains were processed as above.

EM. After intracardiac perfusion of deeply anesthetized animals with 2.5% glutaraldehyde and 2% PFA in 0.1 M sodium cacodylate buffer (pH 7.4), brain tissue was dissected, rinsed, dehydrated in a series of ethanol dilutions (50–100%), and embedded in epoxy resin (Embed 812; Electron Microscopy Sciences). Ultrathin sections (60 nm) were cut on a Reichert ultramicrotome and collected on Formvar- and carbon-coated grids. The samples were stained with 2% uranyl acetate and lead citrate and examined on a Philips Tecnai 12 BioTWIN electron microscope (FEI Co.). Images were captured digitally using a charged-coupled device (CCD) camera (Morada; Soft Imaging System).

Astrocytic Cell Cultures. Astrocytic primary cultures were established as previously described (11). Briefly, neonatal brains (P3) were removed and placed in sterile, ice-cold DMEM/F12 containing 20% FBS. Whole neocortices were dissected, and cortical sheets were further dissected free of meninges, minced with forceps, and forced through a 40-μm nylon mesh (#35230; Beckton-Dickinson). The filtrate was then passed through a 10-μm nylon mesh (part number CMN0010; Small Parts). The resulting single-cell suspension (from each brain) was diluted in DMEM/F12 containing 20% FBS, 100 U/mL penicillin, and 100 μg/mL streptomycin and plated onto T-75 tissue culture flasks that had been precoated with 0.01 mg/mL poly-L-ornithine hydrobromide (Sigma). After 3 d, the medium was changed to DMEM/F12 containing 20% FBS. After 10–14 d, the astroglial cells formed a confluent monolayer. At this point, the resulting cultures were composed of more than 95% astrocytes, as assessed by GFAP immunofluorescence and immunoblotting of lysates. Astrocytes were used at the first passage for all experiments. Control cultures were established from neonates of different genotypes ($Ccm3^{lox/+}$, $Ccm3^{lox/lox}$, or *Gfap*-Cre;$Ccm3^{lox/+}$) that behaved indistinguishably.

In Vitro Assays. To assess apoptosis, astrocytes were treated with cycloheximide (20 μg/mL) (12). Cells were harvested at different time points after treatment and counted using a hemocytometer. For immunoblot analyses, cell lysates were prepared at different time points (as indicated) after treatment. For flow cytometry, astrocytes were stained with annexin V and propidium iodide (TACS Annexin V-FITC apoptosis detection kit; R&D Systems). For the proliferation curve, astrocytes were seeded in six-well plates and harvested at different time points, and cell numbers were counted using a hemocytometer. Cell viability was measured using the 3-(4,5-dimethylthiazol-2-yl)-2,5-diphenyl tetrazolium (MTT) assay. Briefly, astrocytes were seeded in 96-well plates, and MTT was added at different time points (24, 48, and 72 h) at a final concentration of 0.5 mg/mL for 4 h; cells were subsequently lysed in DMSO, and MTT formazan was measured by absorbance at 550 nm using a microplate reader.

Isolation of Brain Endothelial Cells. Primary endothelial cells were isolated from 4-wk-old *Gfap-Cre* and control littermates using a protocol similar to that previously described (13). For each brain endothelial cell prep, neocortices dissected free of meninges from four mice were pooled.

Statistical Analyses. Results are expressed as mean ± SD. Comparisons between groups were analyzed by *t* test. P values < 0.05 were considered statistically significant.

Sulfo-NHS-Biotin Injection. Mice were anesthetized using injectable anesthetics (100 mg/kg ketamine and 10 mg/kg xylazine), intracardially perfused with PBS, and then, perfused with freshly prepared cell surface biotinylation solution (0.5 mg/g body weight diluted in PBS containing 1 mM $CaCl_2$; EZ-link Sulfo-NHS-biotin, #21217; Thermo Scientific) followed after 5 min with 4% PFA. Brains were extracted, cryoprotected in 30% sucrose/PFA, and sectioned. Biotinylated proteins on the luminal surface of the vasculature were detected by streptavidin coupled with alkaline phosphatase and subsequent alkaline phosphatase histochemistry.

Vessel Density. The vascular network was visualized after Sulfo-NHS-biotin injection. Vessel segments per captured image (Zeiss AxioImager with a 10× objective; image field is ~0.55 mm^2) were counted for four to eight images per brain by a blinded investigator. Images were taken from 36-μm coronal sections in the dorsomedial cortex of mutant mice and littermate controls at various ages. When vessels gave off multiple branches, each branch was counted as one additional vessel. Vessel density reflects vessels with sulfo-NHS-biotin staining. Density values for each brain were averaged. A two-tailed Student *t* test, assuming equal variation, was performed to determine the significance of the decrease in vessel density of mutants relative to controls.

RNA Sequencing. Three lesions (representing three biological replicates) were microdissected from the cortical surface of three independent *Emx1-Ccm3* animals (aged 7 mo) and processed for RNA-sequencing (RNA-seq) as follows. RNA was isolated using the RNeasy MinElute kit (Qiagen). The quality of the RNA was evaluated by A260/A280 ratio and electrophoresis on an Agilent Bioanalyzer (Agilent Technologies). RNA (ranging between 7.7 and 40 ng) was amplified using the Ovation RNA-Seq system (NuGEN) before library preparation. The sequencing library was prepared using the mRNA Seq Kit supplied by Illumina according to the manufacturer's protocol. Briefly, mRNA was isolated from total RNA using oligo dT on magnetic beads. The mRNA was then fragmented at 94 °C and converted into double-

stranded cDNA. After polishing of the cDNA ends and addition of adenine bases at the 3′ ends, specific adaptors supplied by Illumina were ligated. The adaptor ligated DNA was amplified by 15 cycles of PCR. The amplified DNA was then purified on the Qiagen PCR purification kit. The insert size and DNA concentration of the sequencing library were determined on an Agilent Bioanalyzer. After cluster generation by isothermal solid-support bridge amplification, one lane of single-read sequencing was performed for each experiment at a read length of 74 bp on the Genome Analyzer IIx (Illumina) according to the manufacturer's protocol. Image analysis and base calling were performed by the Illumina pipeline version 1.5 with default parameters installed on the Yale High-Performance Computing Cluster. Cluster generation and error rates were also evaluated using the pipeline. We next aligned reads to the mouse genome, *Mus musculus* MM9, using Bowtie (14) as implemented in TopHat (15). The splice junctions were mapped by TopHat using the prebuilt splice junction library provided by Trapnell et al. (15). We used Cufflinks (16) to assemble transcripts using RefSeq as the reference list. For quantification of expression level, fragments per kilobase of exon per million fragments mapped (FPKM) values were calculated using Cufflinks.

1. He Y, et al. (2010) Stabilization of VEGFR2 signaling by cerebral cavernous malformation 3 is critical for vascular development. *Sci Signal* 3:ra26.
2. Zhuo L, et al. (2001) hGFAP-cre transgenic mice for manipulation of glial and neuronal function in vivo. *Genesis* 31:85–94.
3. Tronche F, et al. (1999) Disruption of the glucocorticoid receptor gene in the nervous system results in reduced anxiety. *Nat Genet* 23:99–103.
4. Gorski JA, et al. (2002) Cortical excitatory neurons and glia, but not GABAergic neurons, are produced in the Emx1-expressing lineage. *J Neurosci* 22:6309–6314.
5. Sclafani AM, et al. (2006) Nestin-Cre mediated deletion of Pitx2 in the mouse. *Genesis* 44:336–344.
6. Malatesta P, et al. (2003) Neuronal or glial progeny: Regional differences in radial glia fate. *Neuron* 37:751–764.
7. Theis M, et al. (2003) Accelerated hippocampal spreading depression and enhanced locomotory activity in mice with astrocyte-directed inactivation of connexin43. *J Neurosci* 23:766–776.
8. Eckardt D, et al. (2004) Spontaneous ectopic recombination in cell-type-specific Cre mice removes loxP-flanked marker cassettes in vivo. *Genesis* 38:159–165.
9. Tanriover G, et al. (2008) PDCD10, the gene mutated in cerebral cavernous malformation 3, is expressed in the neurovascular unit. *Neurosurgery* 62:930–938.
10. Tole S, Christian C, Grove EA (1997) Early specification and autonomous development of cortical fields in the mouse hippocampus. *Development* 124:4959–4970.
11. Hertz L, Peng L, Lai JC (1998) Functional studies in cultured astrocytes. *Methods* 16: 293–310.
12. Tsuchida T, Kato T, Yamada A, Kawamoto K (2002) Cycloheximide induces apoptosis of astrocytes. *Pathol Int* 52:181–185.
13. Allport JR, et al. (2002) Neutrophils from MMP-9- or neutrophil elastase-deficient mice show no defect in transendothelial migration under flow in vitro. *J Leukoc Biol* 71:821–828.
14. Langmead B, Trapnell C, Pop M, Salzberg SL (2009) Ultrafast and memory-efficient alignment of short DNA sequences to the human genome. *Genome Biol* 10:R25.
15. Trapnell C, Pachter L, Salzberg SL (2009) TopHat: Discovering splice junctions with RNA-Seq. *Bioinformatics* 25:1105–1111.
16. Trapnell C, et al. (2010) Transcript assembly and quantification by RNA-Seq reveals unannotated transcripts and isoform switching during cell differentiation. *Nat Biotechnol* 28:511–515.

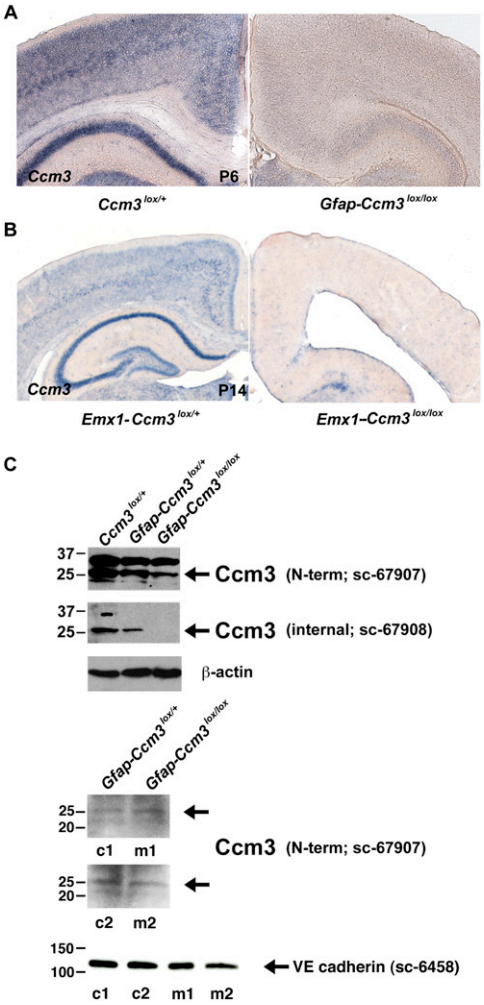

Fig. S1. Loss of *Ccm3* expression in *Ccm3* neural mutants. (*A*) In situ hybridization for *Ccm3* in coronal sections of P6 $Ccm3^{lox/+}$ control and *Gfap-Ccm3* mutant littermates. (*B*) In situ hybridization in coronal sections of P14 *Emx1-*$Ccm3^{lox/+}$ control and *Emx1-*$Ccm3^{lox/lox}$ mutant littermates. In the mutant brains, *Ccm3* mRNA expression is abolished in neural cells of the *Gfap* and *Emx1* lineages, respectively. Results are representative of multiple (greater than eight) independent observations. (*C*) Immunoblot analyses of total brain lysates (*Upper*) for CCM3 using two different antibodies that recognize either N-terminal domain (N-term, #sc-67907; Santa Cruz Biotechnologies) or internal (#sc-67908; Santa Cruz Biotechnologies) epitopes in CCM3. Representative control ($Ccm3^{lox/+}$ and $Gfap\text{-}Ccm3^{lox/+}$) and mutant ($Gfap\text{-}Ccm3^{lox/lox}$) samples. Results are representative of three independent experiments. Immunoblot analyses of brain primary endothelial cell lysates (*Lower*) for CCM3. Representative control ($Gfap\text{-}Ccm3^{lox/+}$) and mutant ($Gfap\text{-}Ccm3^{lox/lox}$) samples (two independent experiments). Each experiment consisted of one control (c1 or c2) and one mutant (m1 or m2) sample; each sample represents endothelial cells isolated from combined neocortices of four animals.

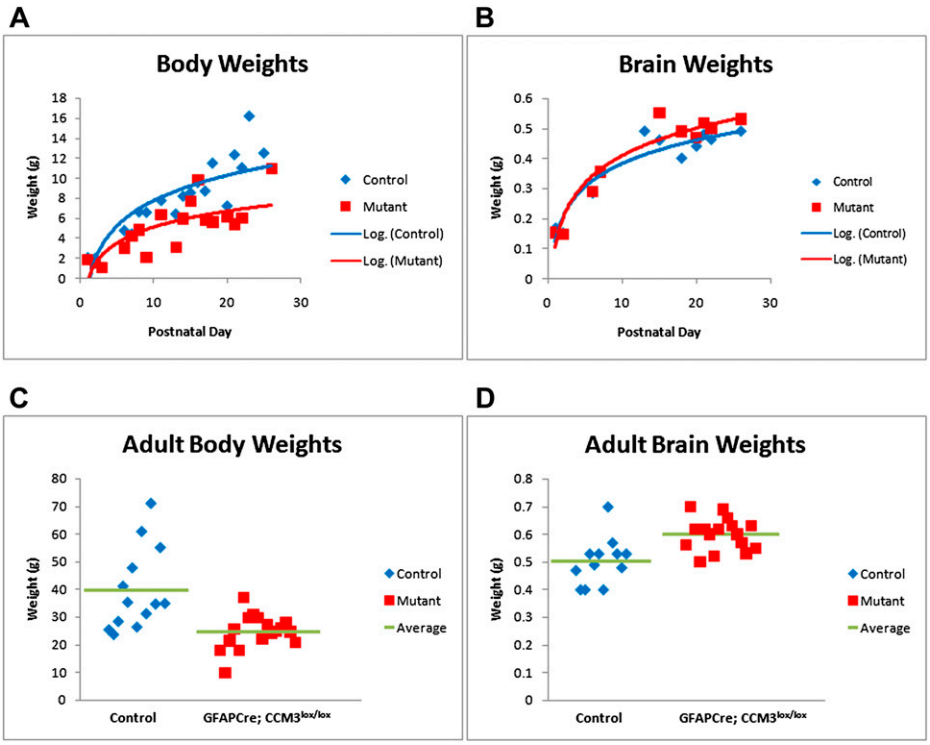

Fig. S2. Body and brain weights of *Gfap-Ccm3* mutant and control littermates. (*A*) Body weights of P0–P26 littermates. (*B*) Brain weights of P0–P26 littermates. (*C*) Body weights of adult *Gfap-Ccm3* survivors and control littermates (5 wk to 12 mo). (*D*) Brain weights of adult *Gfap-Ccm3* survivors and control littermates (5 wk to 12 mo). Brains were dissected and weighed after intracardiac perfusion with 4% paraformaldehyde.

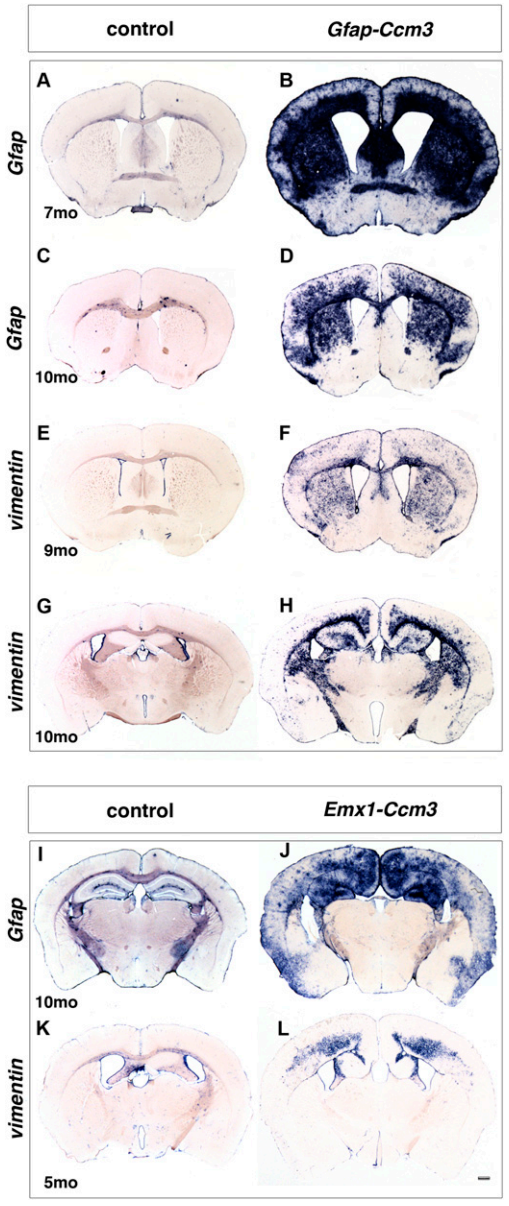

Fig. S3. Extensive astrogliosis in *Gfap-Ccm3* adult survivors (*A–H*) and *Emx1-Ccm3* adult mice (*I–L*). In situ hybridization for *Gfap* (*A–D*, *I*, and *J*) and *vimentin* (*E–H*, *K*, and *L*), encoding intermediate filament proteins, whose up-regulation is the hallmark of activated astrocytes (1, 2). Results are representative of multiple (>20) paired observations. (Scale bar: *A–L*, 50 μm.)

1. Ridet JL, Malhotra SK, Privat A, Gage FH (1997) Reactive astrocytes: Cellular and molecular cues to biological function. *Trends Neurosci* 20:570–577.
2. Pekny M, Nilsson M (2005) Astrocyte activation and reactive gliosis. *Glia* 50:427–434.

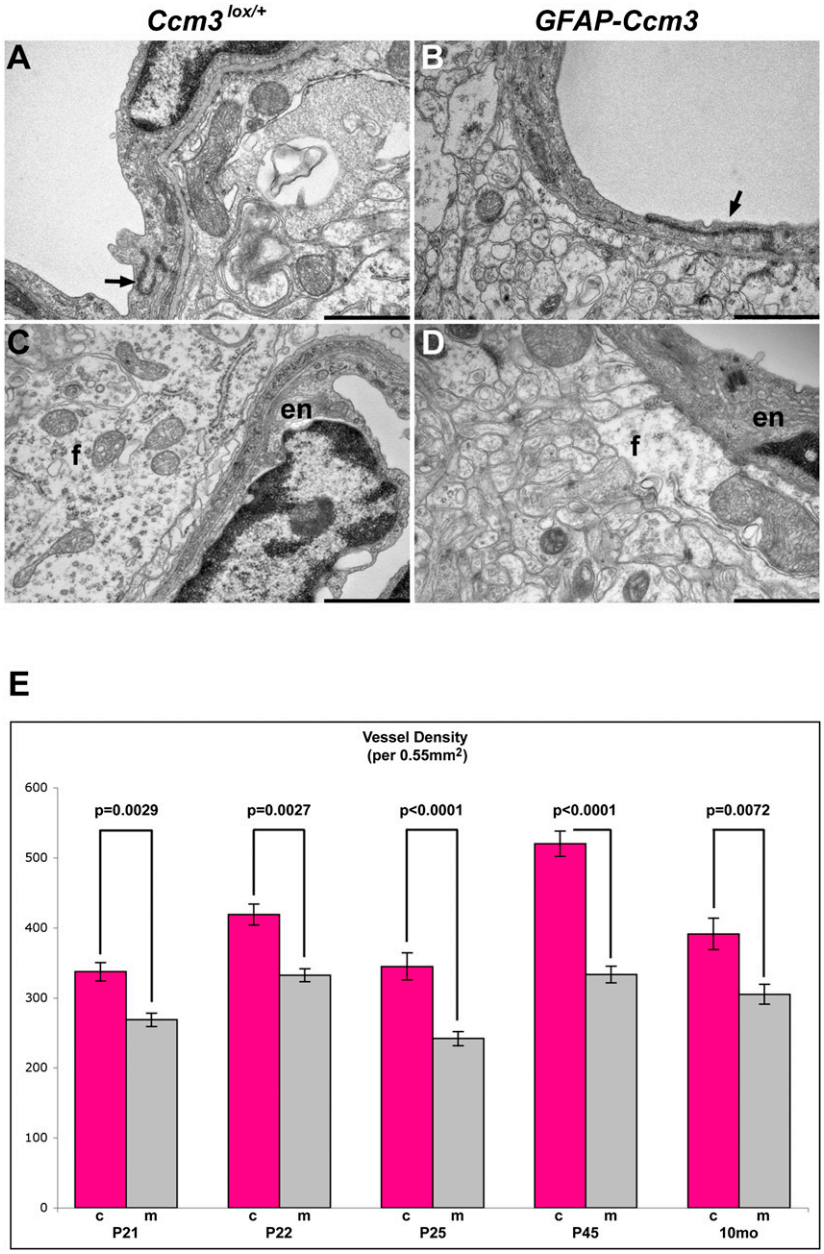

Fig. S4. Ultrastructural morphology of cerebral cortical vessels in young (P18) *Ccm3*$^{lox/+}$ (control) and *Gfap-Ccm3* (mutant) animals. (*A* and *B*) Tight junctions (arrows) between adjacent endothelial cells form in the cerebrovasculature of control and mutant animals. (*C* and *D*) In control and mutant littermates, endothelial foot processes (f) abutting cerebral vessels seem normal. Endothelial cells (en) with partially visible nuclei are shown in both panels. Results are representative of three paired observations. (Scale bars: *A–D*, 1 mm.) (*E*) Vessel density was determined in control (c) and *Gfap-Ccm3* (m, mutant) littermates at different developmental stages as indicated in the figure (*Materials and Methods*). In mutant animals, vessel density was significantly decreased. Results of three paired observations are shown; for each pair, all vessels in four to eight analogous fields of dorsomedial cortex were counted. Values represent means ± SEM.

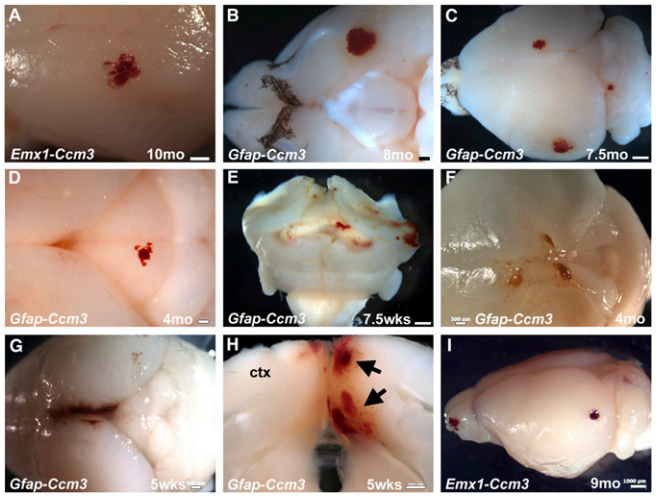

Fig. S5. Vascular lesions in adult animals with neural deletion of *Ccm3*. (*A–I*) Lesions that resemble human cavernomas develop in brain of *Gfap-Ccm3* (*B–H*) and *Emx1-Ccm3* (*A* and *I*) animals. The age of the animals is indicated on each panel. Single (*A*, *B*, and *D*) or multiple (*C* and *E–I*) lesions within the same brain were observed that were predominantly superficial; an example of lesions (arrows) developing within the parenchyma [in the cerebral cortex (ctx)] is shown in *H* on a coronal section of a brain from a *Gfap-Ccm3* animal. Lesions located in lateral cortex (*A*), ventral forebrain (*B*), dorsal and lateral forebrain and midbrain (*C*), midbrain (superior colliculus; *D*), cerebellum (*E*), dorsal cortex (*F*), dorsomedial cortex (*G*), and olfactory bulb and lateral posterior cortex (*I*) are shown. (Scale bars: *A* and *F–H*, 500 μm; *B–E*, 200 μm; *I*, 1,000 μm.)

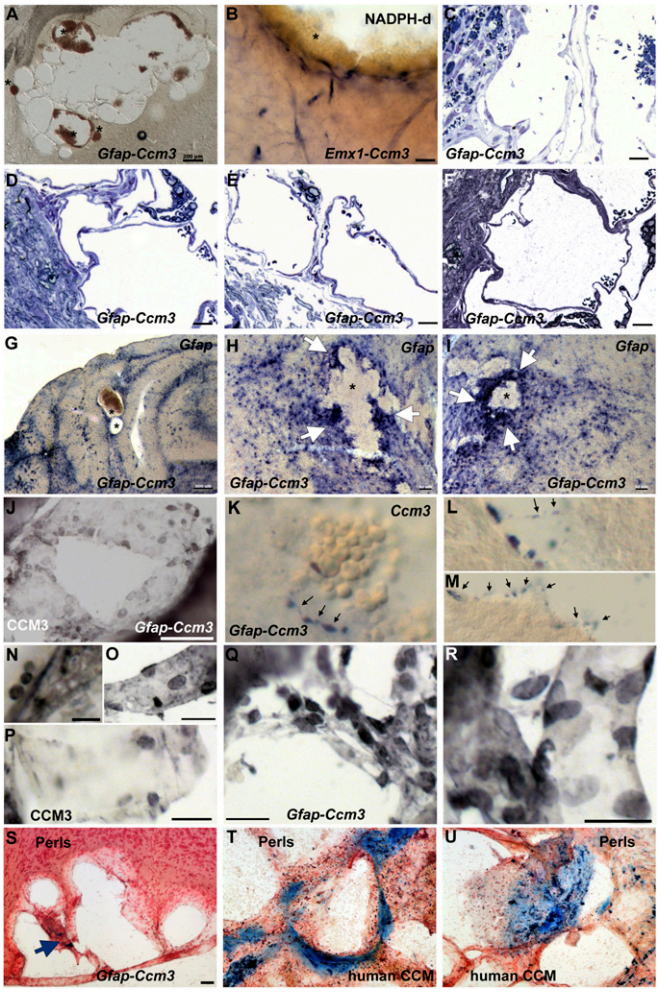

Fig. S6. Fine structure of vascular lesions. (*A*) Low-magnification view of a freshly prepared untreated section (36 μm) of a deep lesion in the cerebellum of a 10-mo-old *Gfap-Ccm3* animal. Note the dilated vascular channels, some of which still contain blood (asterisks). (*B*) NADPH-diaphosase histochemical staining [nitric oxide synthase (NOS) activity] of a lesion from a 9-mo-old *Emx1-Ccm3* animal. Asterisk indicates blood within the dilated lumen of the lesion. (*C–F*) Toluidine blue staining of semithin (0.5- to 0.7-μm) sections of lesions from four *Gfap-Ccm3* animals aged 10 (*C*; $n = 1$) and 7 (*D–F*; $n = 3$) mo. The lesions consist of dilated vascular channels lined by a single layer of endothelium. Some erythrocytes are visible within the lesions. (*G–I*) Multiple deep lesions (asterisks) developing in the parenchyma of cerebellum (*G*) and medulla (two lesions; *H* and *I*) of a *Gfap-Ccm3* animal (P24). The sections were treated for *Gfap* mRNA detection by in situ hybridization. Note strong *Gfap* mRNA expression (arrows) in areas immediately surrounding the lesions. (*J–R*) Lesions from *Gfap-Ccm3* animals immunostained for CCM3 (*J* and *N–R*) or analyzed for *Ccm3* mRNA by in situ hybridization (*K–M*). Cells lining the dilated vascular channels express Ccm3. Arrows in *K–M* indicate cells expressing *Ccm3* mRNA along the dilated vascular channels of lesions. Results are representative of three independent observations. (*S–U*) Perls Prussian blue histochemistry on murine (*S*) and human (*T* and *U*) CCM lesions. Hemosiderin rings are absent in a lesion from a 8-mo-old *Gfap-Ccm3* animal (*S*) but are clearly visible in surgically resected human cavernomas (*T* and *U*). Rare hemosiderin deposits (arrow in *S*) are occasionally seen in murine lesions. Results are representative of four independent observations of murine lesions. (Scale bars: *A* and *G*, 200 μm; *B–F* and *O–U*, 20 μm; *H*, *I*, and *J–M*, 50 μm; *N*, 10 μm.)

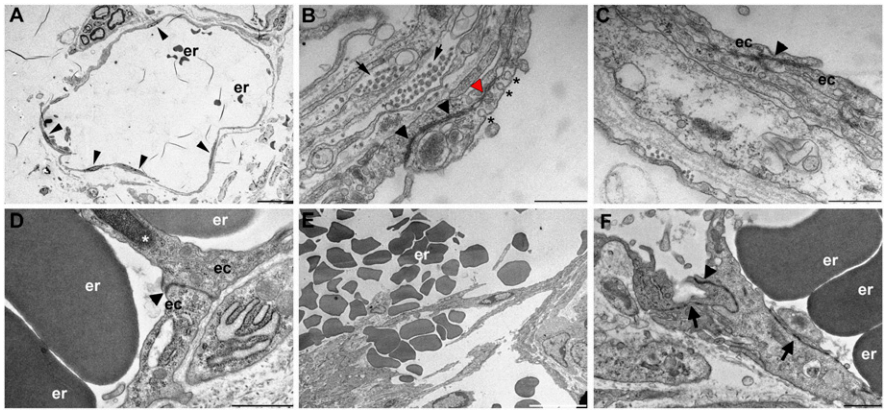

Fig. S7. Transmission electron micrographs of two lesions from two *Gfap-Ccm3* animals aged 7 (*A*–*C*) and 10 (*D*–*F*) mo. (*A*) Low-magnification micrograph showing dilated vascular channels with some erythrocytes (er) retained in the lumen; a single layer of endothelial cells lines the vascular channel (endothelial cell nuclei are indicated by arrowheads), and to the upper left, an axonal bundle in the neuropil is visible. (*B*) Tight junctions (arrowheads) in the endothelial cell layer lining the lumen of the lesion. Caveolae (asterisks) are visible in the luminal side of the endothelial cell, and collagen (arrows) is visible in the abluminal side. (*C*) Tight junction (arrowhead) between neighboring endothelial cells (ec). (*D*) Tight junction (arrowhead) between endothelial cells (ec); erythrocytes (er) are in adjacent vascular channels. An endothelial cell nucleus (asterisk) is partly visible. (*E*) Erythrocytes (er) within a lesion. (*F*) Tight junctions (arrowhead) and adherens junctions (arrows) within a lesion. (Magnifications: *A*, 800×; *B*, *C*, and *E*, 43,000×; *D*, 26,500×; *F*, 16,500×; scale bars: *A*, 20 mm; *B*, *C*, and *E*, 500 nm; *D* and *F*, 1 mm.)

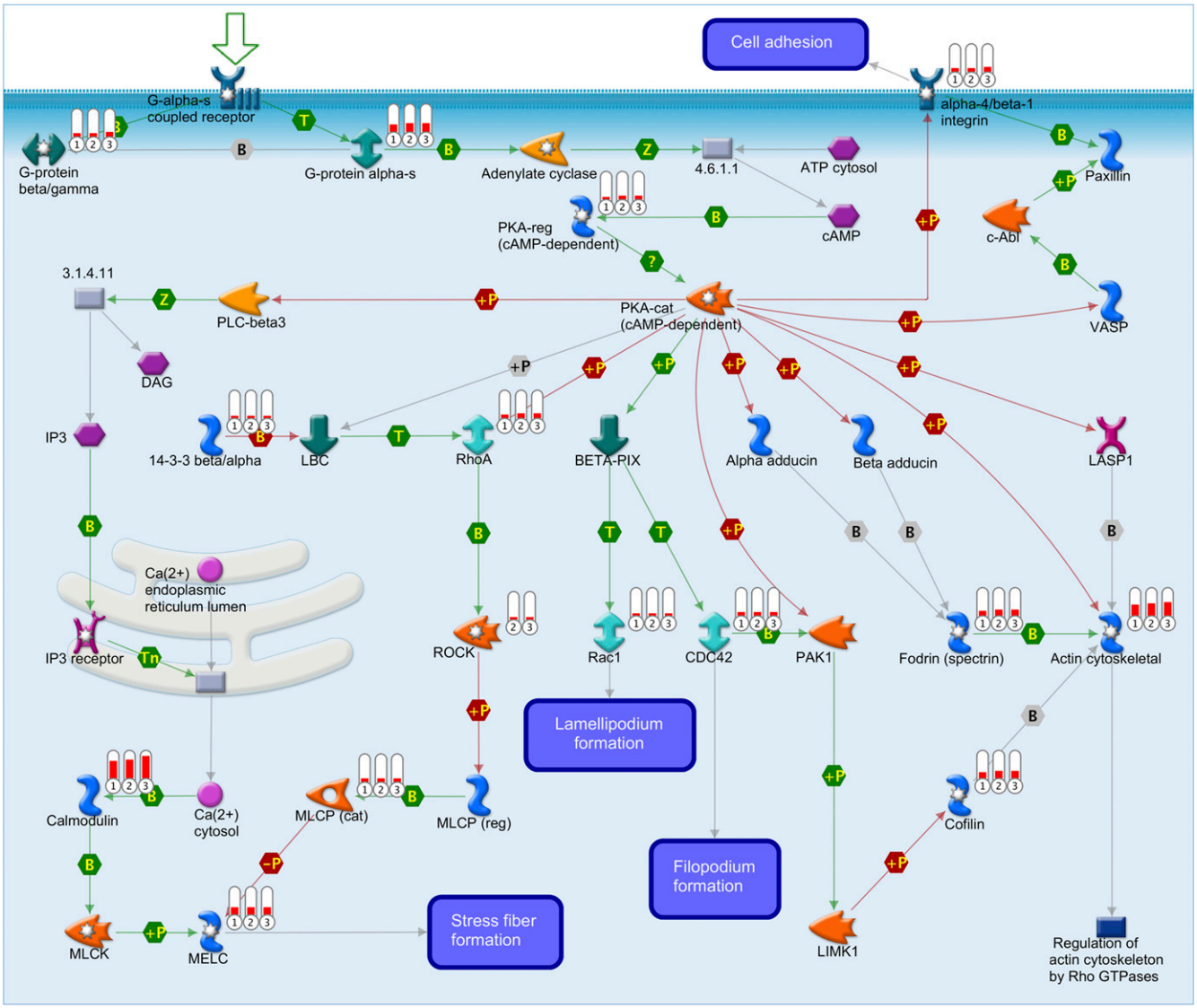

Fig. S8. Pathway analyses of moderately to highly expressed genes identified by RNA-seq of three independent vascular lesions from three *Emx1-Cre* animals indicated the cytoskeletal remodeling pathway to be the most significantly represented pathway. Circles with numbers (1–3) next to pathway objects indicate the abundance of the transcript in each of the lesion samples analyzed; the strength of the red vertical bars indicates levels of abundance.

Table S1. Analysis of *Gfap-Ccm3* and *Emx1-Ccm3* animals

	Age	Sex	Lesion	Other	Figure
Gfap-Ccm3					
1	P23	Male	Multiple	Hydrocephalus	
2	P24	Female	Medulla, deep cerebellum	Hydrocephalus	
3	5 wk	Female	Cortex	Hydrocephalus	5*G*
4	5 wk	Female	Cortex, superficial and deep	Hydrocephalus	5*H*
5	7.5 wk	Male	Two, dorsal cortex	Hydrocephalus	4*G*
6	7.5 wk	?	Multiple	Hydrocephalus	S5*E*
7	2.5 mo	Female	Small, thoracic sc		
8	2.5 mo	Male	Ventral and dorsal brain	Retrieved	
9	3 mo	Male	Cortex	Retrieved	4*F*
10	4 mo	Male	Multiple, cortex	Hydrocephalus	S5*F*
11	4 mo	Male	Ventral midbrain		
12	4 mo	Female	Superior colliculus		S5*D*
13	4.5 mo	Female	Olfactory bulb		
14	5.5 mo	Male	Spinal cord	Retrieved	
15	5.5 mo	Male	Two dorsal ctx, midbrain	Retrieved	
16	7 mo	Male	Olfactory bulb, midbrain		4 *A* and *B*
17	7 mo	Male	Olfactory bulb, sc		S5*A*
18	7 mo	Male	No		
19	7 mo	?	Cerebellum		
20	7.5 mo	Male	Dorsal cortex, midbrain		S5*C*
21	8 mo	Female	Cortex, cerebellum		S5*B*
22	8 mo	Male	No		
23	8.5 mo	Male	No		
24	8.5 mo	Male	No		
25	9 mo	Male	No		
26	10 mo	Male	More than one midbrain, deep		4 *C* and *D*
27	10 mo	Female	No		
28	10 mo	Male	No		
29	11 mo	Male	No		
30	11.5 mo	Female	No		
31	12 mo	Female	No		
Emx1-Ccm3					
1	7 mo	Female	No		
2	7 mo	Female	Two in cortex	RNA-seq	
3	7 mo	Female	Three in cortex	RNA-seq	
4	7 mo	Female	Cortex	RNA-seq	
5	7.5 mo	Female	Cortex		
6	9 mo	Female	Multiple, superficial and deep		S5*I*
7	10 mo	Male	Three in cortex		S5*A*
8	10.5 mo	Male	Yes		
9	11.5 mo	Male	Yes, deep	Retrieved	
10	12 mo	Female	Yes		
11	15 mo	Female	Cortex	Retrieved	4*H*
12	15.5 mo	Male	No		

Gfap-Cre survivors and *Emx1-Cre* adult animals were analyzed. Data include age at endpoint, sex, lesion formation, other features of interest or details on lesion location, and corresponding images in the figures. ctx, cortex; sc, spinal cord.